Article

Cell Stem Cell

Aberrant Lipid Metabolism in the Forebrain Niche Suppresses Adult Neural Stem Cell Proliferation in an Animal Model of Alzheimer's Disease

Graphical Abstract

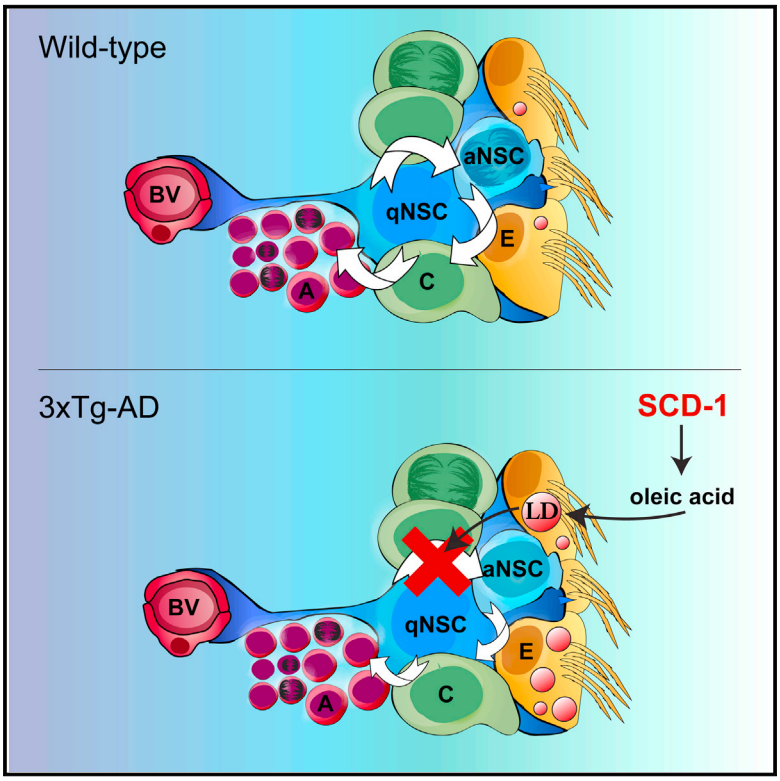

Authors

Laura K. Hamilton, Martin Dufresne, Sandra E. Joppé, ..., Martin Parent, Pierre Chaurand, Karl J.L. Fernandes

Correspondence

karl.jl.fernandes@umontreal.ca

In Brief

Hamilton et al. identify deregulation of niche fatty acid metabolism as a mechanism of disease-induced stem cell impairment. They show that interfering with oleic acid signaling or synthesis rescues NSC proliferation in a mouse model of Alzheimer's, revealing a potential approach to promote NSC-mediated brain function and repair.

Highlights

- Early NSC impairment in 3xTg-AD mice correlates with SVZ niche lipid accumulations
- Similar lipid accumulations are found in the SVZ in postmortem human AD brains
- Accumulating SVZ lipids are locally generated, oleic acid-enriched triglycerides
- Inhibiting oleic acid signaling or synthesis rescues NSC defects in 3xTg-AD mice

Hamilton et al., 2015, Cell Stem Cell *17*, 397–411
October 1, 2015
http://dx.doi.org/10.1016/j.stem.2015.08.001

CellPress

Cell Stem Cell
Article

Aberrant Lipid Metabolism in the Forebrain Niche Suppresses Adult Neural Stem Cell Proliferation in an Animal Model of Alzheimer's Disease

Laura K. Hamilton,[1,2,3] Martin Dufresne,[4] Sandra E. Joppé,[1,2,3] Sarah Petryszyn,[5] Anne Aumont,[1,2,3] Frédéric Calon,[6,7] Fanie Barnabé-Heider,[8] Alexandra Furtos,[4] Martin Parent,[5] Pierre Chaurand,[4] and Karl J.L. Fernandes[1,2,3,*]
[1]Research Center of the University of Montreal Hospital (CRCHUM), Montreal, QC H2X 0A9, Canada
[2]CNS Research Group (GRSNC), Montreal, QC H3T 1J4, Canada
[3]Department of Neurosciences, Faculty of Medicine, Université de Montréal, Montreal, QC H3T 1J4, Canada
[4]Department of Chemistry, Faculty of Arts and Sciences, Université de Montréal, Montreal, QC H3C 3J7, Canada
[5]Department of Psychiatry and Neuroscience, Faculty of Medicine, Université Laval, Quebec City, QC G1J 2G3, Canada
[6]Faculty of Pharmacy, Université Laval, Quebec City, QC G1V 0A6, Canada
[7]CHU-Q Research Center, Quebec City, QC G1V 4G2, Canada
[8]Department of Neuroscience, Karolinska Institutet, 17177 Stockholm, Sweden
*Correspondence: karl.jl.fernandes@umontreal.ca
http://dx.doi.org/10.1016/j.stem.2015.08.001

SUMMARY

Lipid metabolism is fundamental for brain development and function, but its roles in normal and pathological neural stem cell (NSC) regulation remain largely unexplored. Here, we uncover a fatty acid-mediated mechanism suppressing endogenous NSC activity in Alzheimer's disease (AD). We found that postmortem AD brains and triple-transgenic Alzheimer's disease (3xTg-AD) mice accumulate neutral lipids within ependymal cells, the main support cell of the forebrain NSC niche. Mass spectrometry and microarray analyses identified these lipids as oleic acid-enriched triglycerides that originate from niche-derived rather than peripheral lipid metabolism defects. In wild-type mice, locally increasing oleic acid was sufficient to recapitulate the AD-associated ependymal triglyceride phenotype and inhibit NSC proliferation. Moreover, inhibiting the rate-limiting enzyme of oleic acid synthesis rescued proliferative defects in both adult neurogenic niches of 3xTg-AD mice. These studies support a pathogenic mechanism whereby AD-induced perturbation of niche fatty acid metabolism suppresses the homeostatic and regenerative functions of NSCs.

INTRODUCTION

Preservation of stem cell activity within adult tissues is essential for maintaining tissue structure and function. In the brain, experimental inhibition of neural stem cell (NSC) activity leads to deficits in learning and memory, mood, and stress regulation (Imayoshi et al., 2008; Sakamoto et al., 2014; Sakamoto et al., 2011; Snyder et al., 2001). In addition, following neural damage, NSC-derived progeny are re-directed to areas of degeneration, where they are involved in wound healing and cell replacement and can serve as a target for therapeutic manipulations (Benner et al., 2013; de Chevigny et al., 2008; Erlandsson et al., 2011; Kolb et al., 2007). NSC activity decreases naturally during aging and is dysregulated in models of neurodegenerative diseases, suggesting an involvement in aging- and disease-associated cognitive deficits (Bouab et al., 2011; Demars et al., 2010; Hamilton et al., 2010; Hamilton et al., 2013; Lazarov and Marr, 2010; Lazarov et al., 2010). Consistent with this, disturbances in neurogenesis have been reported in Alzheimer's disease (AD) patients (Crews et al., 2010; Perry et al., 2012; Ziabreva et al., 2006) and a range of AD transgenic mouse models (Chuang, 2010; Hamilton et al., 2010). Neural precursor activity can be regulated by gene products involved in both sporadic AD (i.e., ApoE4) (Levi and Michaelson, 2007; Li et al., 2009; Yang et al., 2011) and familial AD (i.e., beta-amyloid, soluble amyloid precursor protein) (Lazarov and Marr, 2010; Smukler et al., 2011). Furthermore, genetic polymorphisms affecting NSC activity can influence AD risk (Nho et al., 2015), while neurogenesis-related genes were identified as a prominently over-represented class of AD risk genes in a recent analysis of published genome-wide linkage, association, and expression studies (Talwar et al., 2014). Thus, dissecting the mechanisms involved in NSC dysregulation could provide new opportunities for preventive and regenerative therapeutic strategies for neurodegeneration.

Recently, lipids have gained attention in the regulation of NSC behavior. In the forebrain subventricular zone (SVZ) niche, lipid metabolism genes are among the major classes of transcriptional differences between quiescent and activated NSCs (Codega et al., 2014). Moreover, in both SVZ and hippocampal dentate gyrus (DG) niches, neural precursors require fatty acid oxidation for proliferation (Chorna et al., 2013; Knobloch et al., 2013; Matsumata et al., 2012; Stoll et al., 2015). NSCs are positioned particularly well in the SVZ to be regulated by environmental lipid signals. Systemic signals can reach NSCs via their contacts with the cerebrospinal fluid (CSF) and SVZ blood vessels (Codega et al., 2014; Mirzadeh et al., 2008; Tavazoie et al., 2008). Ependymal cells are a major source of local signals, constituting approximately 25% of cells within the SVZ niche (Doetsch et al., 1997) and surrounding NSCs in pinwheel

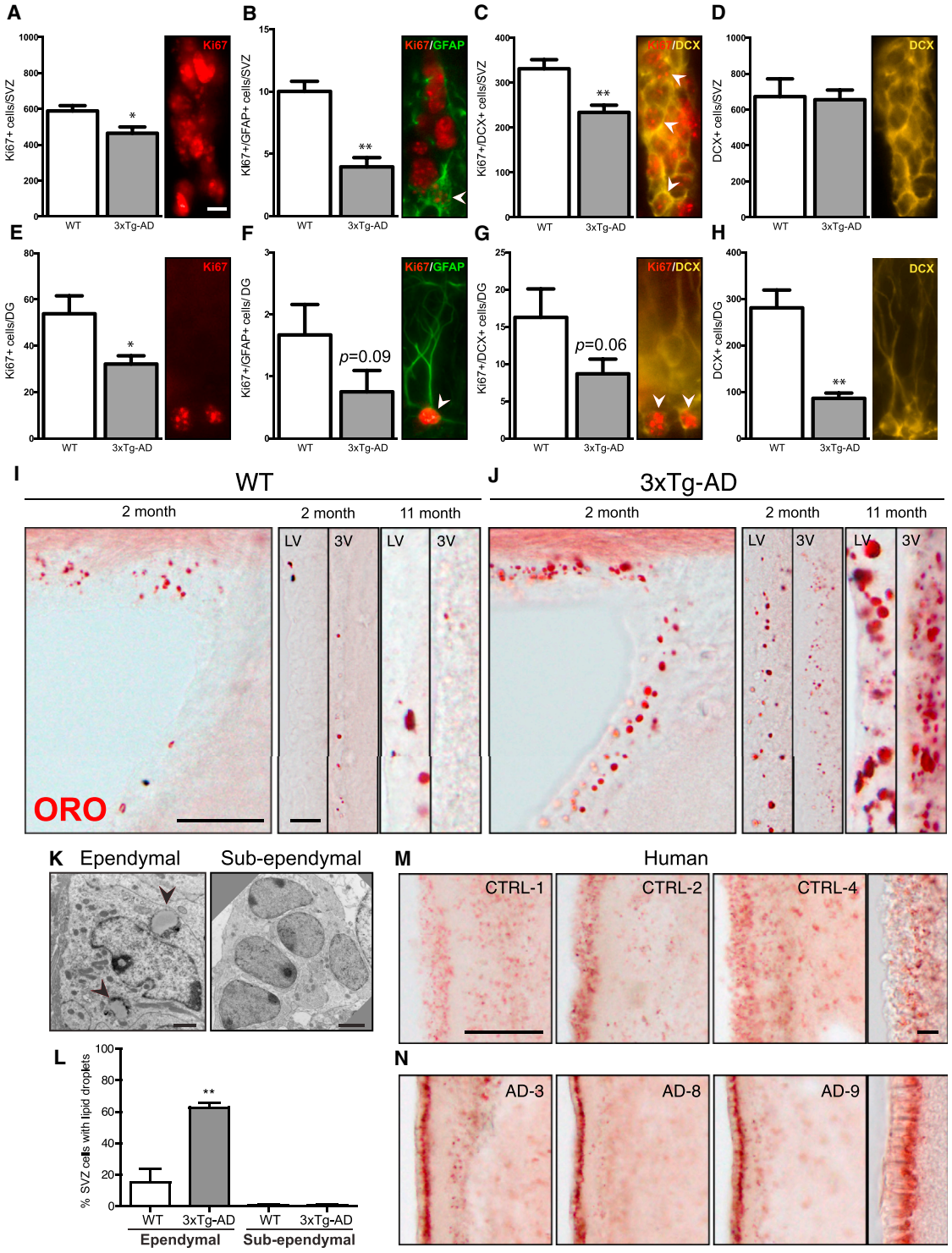

Figure 1. Early Onset of Neurogenesis Defects Correlates with Neutral Lipid Accumulations within Ependymal Niche Cells in the SVZ of AD Mice and Patients

(A–D) Quantification and representative micrographs of Ki67+ proliferating cells (A), Ki67+/GFAP+ proliferating NSCs (B), Ki67+/DCX+ proliferating neuroblasts (C), and DCX+ neuroblasts (D) in the SVZ niche of 2-month-old WT and 3xTg-AD mice (n = 4). Same fields shown in (C) and (D). Unpaired t test.

(E–H) Quantification and representative micrographs of Ki67+ proliferating cells (E), Ki67+/GFAP+ proliferating NSCs (F), Ki67+/DCX+ proliferating neuroblasts (G), and DCX+ neuroblasts (H) in the DG niche of 2-month-old WT and 3xTg-AD mice (n = 4). Same fields shown in (E) and (G). Unpaired t test.

(I and J) ORO staining of coronal sections containing the lateral ventricle (LV) and third ventricle (3V) of 2-month-old and 11-month-old WT (I) and 3xTg-AD (J) mice.

(legend continued on next page)

structures within the walls of the lateral ventricles (Mirzadeh et al., 2008). Ependymal cells provide a critical interface for the exchange of ions, macromolecules, and immune cells between the brain and the circulating CSF, secrete a variety of molecules that regulate NSC activity, and have been identified as sites of lipid synthesis and storage (Bouab et al., 2011; Etschmaier et al., 2011; Hamilton et al., 2010).

Interestingly, AD is associated with both declines in neurogenesis-regulated cognitive processes and aberrations in lipid metabolism. Indeed, lipid accumulations were one of the five original AD-associated tissue pathologies reported by Alois Alzheimer (Alzheimer, 1907). More recently, links have strengthened between aberrant lipid metabolism and neurodegeneration in AD (Astarita et al., 2011; Fraser et al., 2010; Hussain et al., 2013; Podtelezhnikov et al., 2011; Tanzi, 2012), while epidemiological studies have demonstrated that AD risk factors include peripheral metabolic conditions such as insulin resistance, obesity, and dyslipidemia (Pasinetti and Eberstein, 2008). However, deeper mechanistic insights into the role of abnormal lipid metabolism in AD have been hindered by the technical complexity involved with localizing, identifying, and determining the biological functions of individual lipid species in the brain.

In the present study, we developed methodologies to overcome these limitations, allowing us to uncover a new pathological mechanism in AD. Our results reveal that lipid metabolism defects originating within a major neurogenic niche can disrupt NSC-mediated regeneration and plasticity.

RESULTS

Early Onset of Neurogenesis Defects and AD-Associated Neutral Lipid Accumulations at the Brain-CSF Interface

The triple-transgenic Alzheimer's disease (3xTg-AD) mouse is a unique AD model that accumulates both amyloid plaques and neurofibrillary tangles with age (Oddo et al., 2003). We have previously shown that neural precursor proliferation and neurogenic output are decreased in 3xTg-AD mice at both 11 and 18 months of age (Hamilton et al., 2010). We hypothesized that if suppression at the level of NSCs underlies the defects in neurogenic output, then it should be possible to identify an earlier time window when only proliferating precursors are affected. Consistent with this, multi-stage analysis of SVZ neurogenesis in 2-month-old mice revealed that 3xTg-AD mice already have significant decreases in total Ki67+ cell proliferation (Figure 1A), Ki67+/glial fibrillary acidic protein (GFAP+) proliferating NSCs (Figure 1B), and Ki67+/DCX+ proliferating neuroblasts (Figure 1C), without alterations in the total number of DCX+ neuroblasts (Figure 1D), number of pinwheel units (Figure S1A), or neurospheres (Figure S1B). There was also no significant difference in Ki67+/Iba1+ proliferating microglia (Figure S1C). In the hippocampal DG niche, total Ki67+ (Figure 1E) and total DCX+ (Figure 1H) populations were both significantly decreased, while Ki67+/GFAP+ proliferating NSCs (Figure 1F) and Ki67+/DCX+ proliferating neuroblasts (Figure 1G) showed trends toward decreases that approached statistical significance. The number of Ki67+/Iba1+ proliferating microglia was unchanged (Figure S1D).

Neurogenesis impairments in 3xTg-AD mice occur before amyloid plaques and neurofibrillary tangles (Hamilton et al., 2010), suggesting the involvement of other pathogenic mechanisms. We observed that NSC suppression in 2-month-old 3xTg-AD mice occurred concomitant to a highly specific accumulation of oil red O (ORO)-positive neutral lipid droplets along the entire brain-CSF interface, including the lateral ventricle of the forebrain SVZ niche and the third ventricle of the hypothalamus (Figures 1I and 1J). At 2 months of age, SVZ lipid droplets were statistically significantly increased in 3xTg-AD mice compared to wild-type (WT) mice (Figure S1E), and lipid droplet numbers correlated well with the observed declines in SVZ neurogenesis markers (Figures S1F–S1I). ORO-positive lipid droplets continued increasing with age in 3xTg-AD mice; however, even at 11 months of age, they were never detected outside of the ventricular zone in either WT or 3xTg-AD mice (Figures 1I and 1J). SVZ lipid droplets were found uniquely in ventricle-contacting ependymal cells and did not accumulate in the sub-ependymal populations of neural precursors (Figures 1K and 1L). These data reveal a buildup of lipid droplets within the SVZ niche during the window of preferential NSC inhibition.

We then tested whether aberrant lipid accumulations are present in the SVZ of postmortem human AD brains (Figures 1M and 1N). Remarkably, we found similar lipid accumulations along the lateral ventricles in post-mortem brain tissues from nine AD patients (78.0 ± 2.89 years old) and five age-matched cognitively normal individuals (79.6 ± 5.88 years old) (Figures 1M and 1N; Figures S1E and S1F; Table S1 for patient information). Four of the five controls presented sparse ORO staining of the ependymal layer along the majority of the ventricular wall (Figures 1M and S1J). In contrast, the majority of AD brains showed dense accumulations of ORO at the basal surface of the ependyma (Figures 1N and S1K), with four of the nine presenting a mixture of dense and sparse areas. These data collectively reveal a selective accumulation of lipid droplets along the brain-CSF interface of both human AD brains and 3xTg-AD mice, and at least in 3xTg-AD mice, this accumulation coincides with impaired NSC function during early adulthood.

Accumulating AD-Associated Lipids Are Triglycerides Enriched with Oleic Acid

Lipid droplets are lipid-rich organelles composed of neutral lipids such as fatty acids, triglycerides, and sterols (Martin and Parton, 2006). To identify the classes of lipids accumulating within the SVZ niche, we developed an imaging mass spectrometry (IMS)-based lipidomics strategy. IMS is a unique form of mass

(K and L) Representative micrographs (K) and quantifications (L) of lipid droplets (arrowheads) in 3xTg-AD ependymal versus sub-ependymal cells (n = 3). One-way ANOVA.

(M and N) ORO staining of transverse sections containing the LV and the SVZ of normal individuals (CTRL) (M) and AD patients (N). Panels at the right show representative higher-magnification images.

The scale bar in (A) (for A–H) represents 5 μm, in (I) (for I and J) and (M) (for M and N) represents 100 and 10 μm, in (K) represents 1 and 2 μm. Error bars represent mean ± SEM. *$p \leq 0.05$ and **$p \leq 0.005$. See also Figure S1 and Table S1.

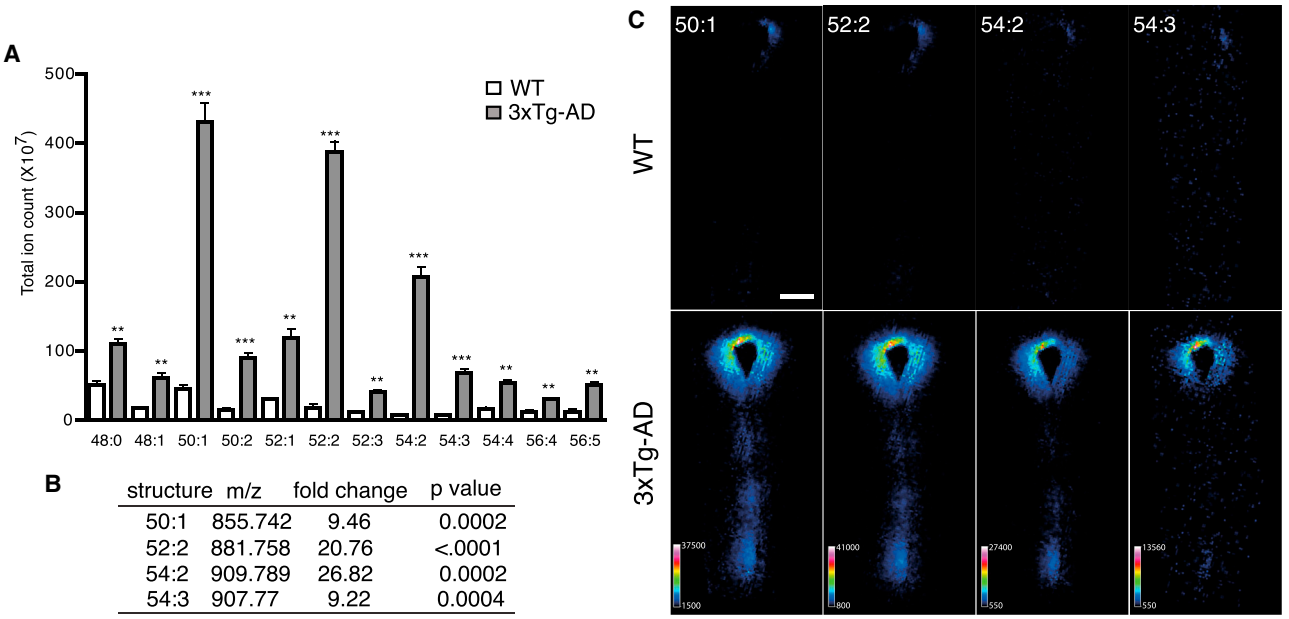

structure	m/z	fold change	p value
50:1	855.742	9.46	0.0002
52:2	881.758	20.76	<.0001
54:2	909.789	26.82	0.0002
54:3	907.77	9.22	0.0004

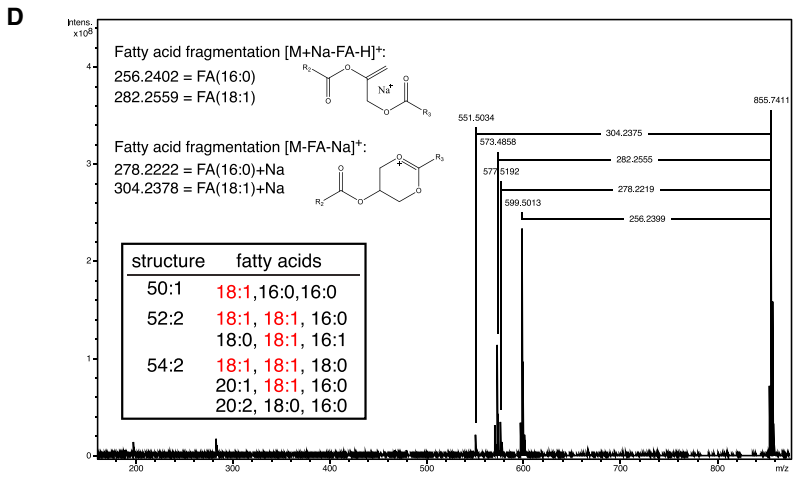

structure	fatty acids
50:1	18:1,16:0,16:0
52:2	18:1, 18:1, 16:0 18:0, 18:1, 16:1
54:2	18:1, 18:1, 18:0 20:1, 18:1, 16:0 20:2, 18:0, 16:0

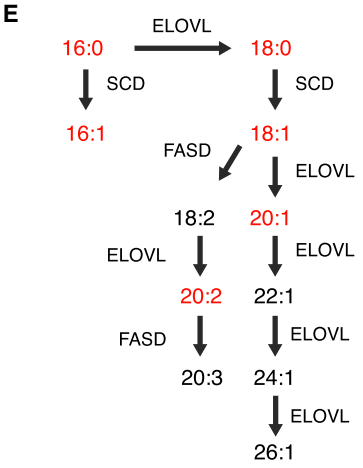

Figure 2. Accumulating AD-Associated Lipids Are Triglycerides Enriched in OA

(A–C) IMS showing the 12 triglycerides that accumulate surrounding the lateral ventricle of 5-month-old 3xTg-AD mice. (A) Structures (total carbon-to-unsaturation ratio) of the 12 enriched triglycerides with their associated total ion counts. (B) Table of m/z ratios and fold changes of the 4 most enriched triglycerides (50:1, 52:2, 54:2, and 54:3). (C) Representative ion density maps. Unpaired t test.

(D) Tandem mass spectrometry of the three major triglycerides (50:1, 52:2, and 54:2) to identify their fatty acid side chains. The fractionation pattern from the sodium-adducted triglyceride 50:1 is shown. The inset table summarizes the combined fractionation patterns of the three major triglycerides, showing a predominant enrichment of OA (red).

(E) Fatty acid biosynthesis pathway involved in the production and subsequent processing of OA (18:1). Fatty acids identified as enriched in the 3xTg-AD SVZ are shown in red. Enzymes involved at each step are shown, and include the SCD, ELOVL, and FASD gene families.

The scale bar in (C) represents 200 μm. Error bars represent mean ± SEM. *$p \leq 0.05$, **$p \leq 0.005$, and ***$p \leq 0.0005$. See also Figure S2.

spectrometry that employs laser desorption-ionization to collect mass spectra data at high-resolution intervals across a tissue section, thereby revealing the spatial distribution of individual biomolecules within the unperturbed tissue architecture. IMS revealed that lipid accumulations in the SVZ niche are selectively enriched in triglycerides. Twelve distinct triglycerides were found to be increased by 2- to 27-fold in the SVZ niche of 3xTg-AD mice compared to strain controls (Figure 2A). The four largest increases occurred in triglycerides having structures of 50:1, 52:2, 54:2, and 54:3 (total carbon-to-unsaturation ratio) (Figure 2B), and IMS ion density maps illustrated a specific enrichment of these triglycerides along the ventricular borders (Figures 2C and S2A). Conversely, cholesterol content in the SVZ was unchanged (Figure S1B).

Triglycerides are composed of a glycerol head group with three fatty acid side chains. Because individual fatty acids have distinctive effects on energy metabolism, intra- and inter-cellular signaling, gene expression, and membrane properties, we identified the constituent fatty acids of the accumulating ependymal triglycerides using tandem mass spectrometry. Ionization of the three most increased triglycerides yielded predictions of oleic acid (OA) (18:1), palmitic acid (16:0), stearic acid (18:0), palmitoleic acid (16:1), eicosenoic acid (20:1), and eicosadienoic acid (20:2) side chains in an approximately 7:5:3:1:1:1 ratio (Figure 2D). Interestingly, these fatty acids are closely related within a common fatty acid biosynthetic pathway (Figure 2E). Together, these data reveal a panel of AD-associated triglycerides that accumulate at the brain-CSF interface and that are enriched in OA.

Short-Term ICV Infusion of OA Recapitulates Lipid Droplets and AD-Associated Triglycerides but Does Not Affect SVZ Neurogenesis

Because OA was the major fatty acid accumulating in the SVZ niche, we investigated the consequences of increasing local OA levels in the SVZ of WT mice. OA administration to WT mice for 7 days by direct intracerebroventricular (ICV) infusion resulted in the formation of ORO-positive ependymal lipid droplets that closely resembled those of 3xTg-AD mice and human AD patients (Figures 3A and 3B). Moreover, IMS showed a concomitant increase in AD-associated triglycerides (Figure 3C). To determine whether this was a direct or indirect consequence of OA administration, we traced the incorporation of the infused OA with a sensitive in vivo metabolic labeling procedure that uses OA comprised entirely of heavy ^{13}C (^{13}C OA) (Figures 3D–3F). Comparison of IMS spectra between ^{13}C OA and regular ^{12}C OA revealed that OA infusion into WT mice is sufficient to generate virtually all AD-associated triglycerides. For example, ^{13}C OA shifted the triglyceride 50:1 by exactly 18.060 atomic units (incorporation of one OA side chain), the triglyceride 52:2 by 18.060 and 36.120 atomic units (incorporation of up to two OA side chains) (Figures 3D–3F), the triglyceride 54:2 by 18.060 and 36.120 atomic units (incorporation of up to two OA side chains) and the species 54:3 by 18.060, 36.120, and 54.180 atomic units (incorporation of up to three OA side chains). Uptake of ^{13}C OA into each of the 12 AD-associated triglycerides is summarized in Figure 3F and shows that 11 of the 12 AD-associated triglycerides are replicated in WT mice simply by ICV infusion of OA. These metabolic labeling experiments also demonstrated that some AD-associated triglycerides contained ^{13}C OA that had been elongated (56:4 and 56:5), reduced (52:2 and 52:3), saturated (52:2 and 54:2), and/or desaturated (54:4, 56:4, and 56:5), revealing that OA at the brain-CSF interface can be used as a substrate to locally generate longer chain and polyunsaturated fatty acids.

We then assessed OA's effects on SVZ neurogenesis following this 7-day ICV infusion. Multi-stage analysis of SVZ neurogenesis revealed that there were no changes in any of the SVZ cell populations analyzed (Figures 3G–3M), including total cell proliferation (Figure 3G), proliferating NSCs (Figure 3H), number of pinwheel units (Figure 3I), number of neurospheres grown (Figure 3J), proliferating neuroblasts (Figure 3K), total neuroblasts (Figure 3L), and proliferating microglia or macrophages (Figure 3M). Thus, short-term elevation of a single fatty acid, OA, is sufficient to induce ependymal lipid droplet accumulation and to replicate the AD-associated triglyceride phenotype, but it does not have a generalized inhibitory or toxic effect on the SVZ.

OA Treatment Selectively Suppresses NSC Activity

Little is known about the impact of fatty acids on NSC function. Because the 2- to 3-week in vivo division frequency of NSCs is much longer than the 7-day OA infusion paradigm used earlier, we employed more targeted in vitro and in vivo assays to specifically test whether excess OA negatively regulates NSC activity.

We found that OA concentration is a critical determinant of NSC colony formation in the in vitro neurosphere assay, because doubling the OA concentration was sufficient to convert it from a positive to a negative regulator of neurosphere formation (Figures 4A–4F and S3A–S3D). Neural precursors exposed to elevated OA at the time of initial plating (when neurosphere growth requires NSC activation) generated 50% fewer neurosphere colonies (Figures 4A and 4B). In contrast, neural precursors exposed to the same OA concentration after 4 days in vitro (when neurosphere growth is driven by proliferation of progenitors) were unaffected (Figures 4C and 4D). Consistent with a specific effect on NSCs, neurosphere self-renewal assays showed that when OA and vehicle-treated spheres of equal sizes were dissociated and re-plated under identical neurosphere-forming conditions, there were 20% fewer neurosphere-initiating NSCs in OA-treated neurospheres (Figures 4E and 4F). Flow cytometry (Figure 4G) and immunocytochemistry (Figures 4H and 4I) confirmed that 100 μM OA inhibits division of a sub-population of neural precursors but does not have a generalized impact on either proliferation or cell death. Thus, in vitro, elevated OA levels selectively inhibit NSC proliferation.

The previous data suggested a model in which OA accumulating in ependymal cells acts in a paracrine manner to dysregulate NSC activity. To begin exploring this idea, we first tested whether the SVZ of 3xTg-AD mice releases anti-neurogenic factors by growing WT NSCs in the presence of either 3xTg-AD or WT SVZ whole mounts. We found a 50% decrease in neurosphere number after whole mount co-culture from 3xTg-AD mice (Figure 4J), revealing that the SVZ of 3xTg-AD mice contains factors that inhibit NSC proliferation. Conditioned media from 3xTg-AD whole mounts likewise inhibited the neurosphere number by more than 50% when compared to WT whole mounts (Figure 4J), indicating that this AD-associated inhibitory activity is mediated by soluble rather than contact-mediated mechanisms. Interestingly, the decline in the neurosphere number is similar in magnitude to that observed following 100 μM OA treatment (Figures 4A and 4B). This confirms that soluble factors released from the 3xTg-AD niche inhibit NSC activity.

NSCs only divide once every several weeks in vivo, making it difficult to assess treatment-induced changes in their activity. We therefore employed a well-characterized SVZ regeneration assay to evaluate whether excess OA can suppress NSC activation in vivo. In this model, elimination of proliferating SVZ cells (primarily progenitors and neuroblasts) with the anti-mitotic agent cytosine arabinoside (AraC) results in more synchronized activation of the quiescent NSC pool, which then rapidly repopulates the SVZ niche (Doetsch et al., 1999). After 6 days of infusion of AraC with either OA or vehicle, pumps were removed and the animals were sacrificed 24-hr post-AraC withdrawal (Figures

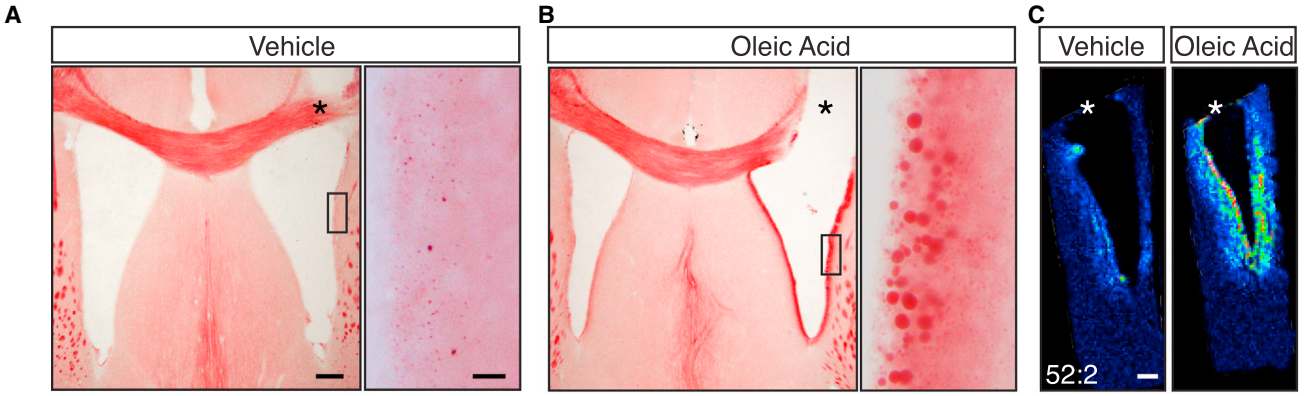

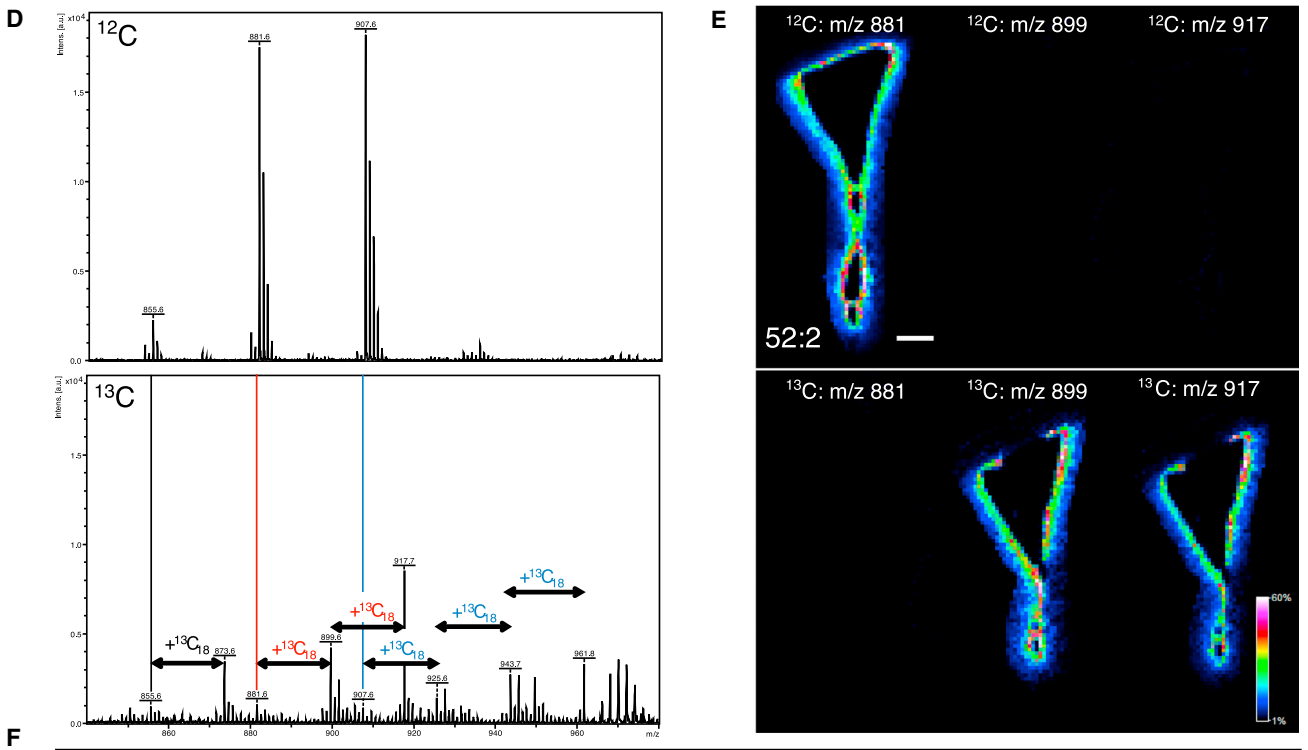

F

Structure	48:0	48:1	50:1	50:2	52:1	52:2	52:3	54:2	54:3	54:4	56:4	56:5
Number of ^{13}C-OA	0	1	1	2	1	2	2	2	3	3	3	3

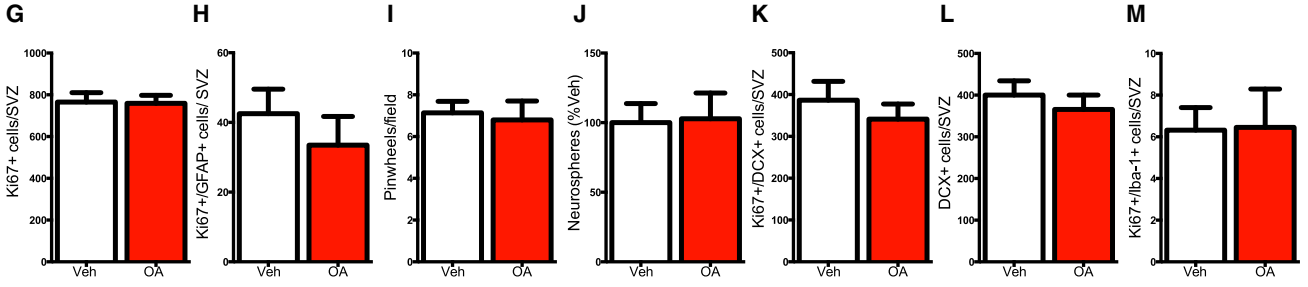

Figure 3. Short-Term ICV Infusion of OA Recapitulates Lipid Droplets and AD-Associated Triglycerides but Does Not Significantly Affect SVZ Neurogenesis

(A and B) ICV infusion of vehicle (n = 4) (A) or OA (n = 4) (B) for 7 days, with boxed areas magnified at the right.

(C) Representative IMS ion density maps following vehicle or OA infusion showing an AD-associated triglyceride that is induced by OA infusion.

(D and E) IMS following metabolic labeling with ^{12}C OA (n = 3) versus ^{13}C OA (n = 3) (D), with sample ion density maps of 52:2 (E).

(legend continued on next page)

4K–4N). No proliferating or post-mitotic neuroblasts were present in the SVZ (data not shown), consistent with previous findings (Doetsch et al., 1999) and validating that the AraC treatment was effective. Quantification revealed that OA inhibited the NSC-mediated recovery, significantly decreasing the total numbers of Ki67+ proliferating cells (Figure 4L) and Ki67+/GFAP+ proliferating NSCs (Figure 4M) when compared to vehicle. There was no significant impact on the numbers of proliferating microglia or macrophages within the SVZ (Figure 4N). Thus, increased OA within the SVZ niche can suppress proliferation of NSCs, adversely impacting their ability to maintain niche homeostasis.

Lipid Metabolism Alterations Occur within the SVZ Niche

The previous data suggested that OA accumulation at the brain-CSF interface is a key mediator of AD-associated NSC impairment. To identify a possible systemic origin of the accumulating OA, we studied the plasma and CSF of 3xTg-AD mice using a liquid chromatography mass spectrometry (LC-MS)-based lipidomic approach (see Experimental Procedures and Figures S4 and S5). However, concentrations of the 12 AD-associated triglycerides and their associated free fatty acids were unchanged between 3xTg-AD mice and their WT controls in both these circulating fluids (Figures 5A and 5B). Moreover, the central versus peripheral lipid profiles of 3xTg-AD mice exhibited differential changes as cholesterol was increased in the 3xTg-AD plasma (Figure S5E) but not within the 3xTg-AD SVZ (Figure S2B). We therefore explored whether lipid metabolism was altered within the SVZ niche.

Gene expression in the microdissected SVZ of 3xTg-AD versus WT mice was compared using a 55,681-probe genome-wide microarray and revealed 993 significantly up- or downregulated genes (fold change $\geq$ 1.4 and $p \leq 0.005$) (Figure 5C). Functional analysis of this dataset identified cellular metabolism (comprising carbohydrate, nucleic acid, amino acid, and lipid metabolism) as one of the top five significantly altered categories, along with neurogenesis-related categories such as cognitive function, cell cycle, and proliferation and cellular differentiation (Figure 5D and Table S2). Manual and database-mediated extraction of lipid-related genes revealed that 142 of the 993 significantly modulated changes (14.3%) were lipid related (Figure 5E and Table S3), including genes implicated in various aspects of fatty acid metabolism (i.e., PLA2, SCD-1, ELOVL7, FABP5, LIPIN2, and NPC1).

Together, these data show that AD-associated triglycerides accumulating in SVZ ependymal cells are unlikely to originate in the periphery, and they identify the SVZ niche as a site of AD-associated alterations in lipid metabolism gene expression.

Hyper-Activation of AKT Signaling Mediates OA-Induced Impairment of NSC Activity

We next investigated ways of interfering with OA-induced NSC impairments. Studies of several peripheral cell types indicate that OA release can modulate AKT activity in target cells (Lee et al., 2014; Shibata et al., 2013; Yun et al., 2006). Consistent with AKT being a possible mediator of OA's effects on NSCs, a single ICV injection of OA into WT mice led to hyper-phosphorylation of AKT within the ipsilateral SVZ within 4 hr (Figures 6A–6C). Similarly, when SVZ neural precursors were cultured using the neurosphere assay, acutely treated with OA, and then lysed after 15 min, 30 min, 1 hr, 2 hr, 4 hr, and 24 hr, an increase in AKT signaling was observed beginning at the 4-hr point (Figures 6D and 6E and data not shown).

To begin testing whether OA-induced hyper-activation of AKT inhibits NSC activity, we used a pharmacological approach to suppress AKT phosphorylation in cultured neurosphere-derived cells (Figures 6D and 6E). This experiment showed that OA on its own increased phosphorylated AKT (pAKT), 12.5 μM of the PI3-kinase inhibitor LY294002 eliminated basal pAKT, and when OA was combined with LY294002, OA normalized pAKT toward control levels (Figures 6D and 6E). OA treatment and LY inhibition did not have a statistically significant effect on phosphorylated extracellular signal-related kinase (pERK) (Figure 6D). Based on these biochemical data, we hypothesized that if OA-induced hyper-phosphorylation of AKT mediates its inhibition of NSCs, then simultaneous inhibition of pAKT with LY294002 should rescue OA's inhibition of neurosphere formation. Indeed, when neurospheres were passaged into the medium containing OA, LY294002, or OA+ LY294002, OA reduced the neurosphere number by 50% (as in our previous experiments), LY294002 dose-dependently inhibited the neurosphere number, and remarkably, OA's negative effect on neurosphere formation was converted to a positive effect when combined with LY294002 (i.e., an increased neurosphere number compared to vehicle) (Figures 6F and 6G). These data implicate AKT signaling as an important effector of OA's effects on NSCs in vitro and suggest that NSCs require an optimal level of AKT signaling: excess OA under normal conditions leads to a detrimental hyper-stimulation of AKT activity, whereas excess OA under conditions of insufficient AKT signaling leads to a beneficial normalization of AKT activity.

We then used an adult brain electroporation approach (Barnabé-Heider et al., 2008) to genetically target ventricle contacting GFAP-expressing NSCs, allowing us to determine whether AKT also mediates OA's effects on NSC proliferation in vivo. A plasmid encoding GFAP-cre was electroporated into the ventricle walls of adult R26-flox-stop-flox-EYFP mice to induce the expression of EYFP in GFAP+ NSCs and their progeny. The GFAP-cre plasmid was co-electroporated with plasmids encoding either kinase-dead AKT (KD-AKT) or empty vector (EV). Immediately following electroporation, 7-day mini-osmotic pumps were implanted for ICV infusion of either vehicle or OA to test the effects of OA on the electroporated ventricle-contacting NSCs (Figures 6H and 6I). Consistent with our previous data, quantification of the EYFP+ cells after 7 days showed that OA

(F) Table summarizing the number of ^{13}C OA chains incorporated into each AD-associated triglyceride.

(G–M) 7-day vehicle (n = 5) or OA (n = 5) infusion for quantification of Ki67+ proliferating cells (G), Ki67+/GFAP+ proliferating NSCs (H), whole-mount pinwheel units per field (n = 3 vehicle or n = 4 OA) (I), neurosphere number (n = 3 vehicle or n = 4 OA) (J), Ki67+/DCX+ proliferating neuroblasts (K), DCX+ neuroblasts (L), and Ki67+/Iba-1+ proliferating microglia (M) in the SVZ niche. Unpaired t test.

Scale bars in (A) (for A and B) represent 200 and 10 μm and in (C) and (E) represent 200 μm. Error bars represent mean ± SEM. * in (A)–(C) denotes the ipsilateral injection side.

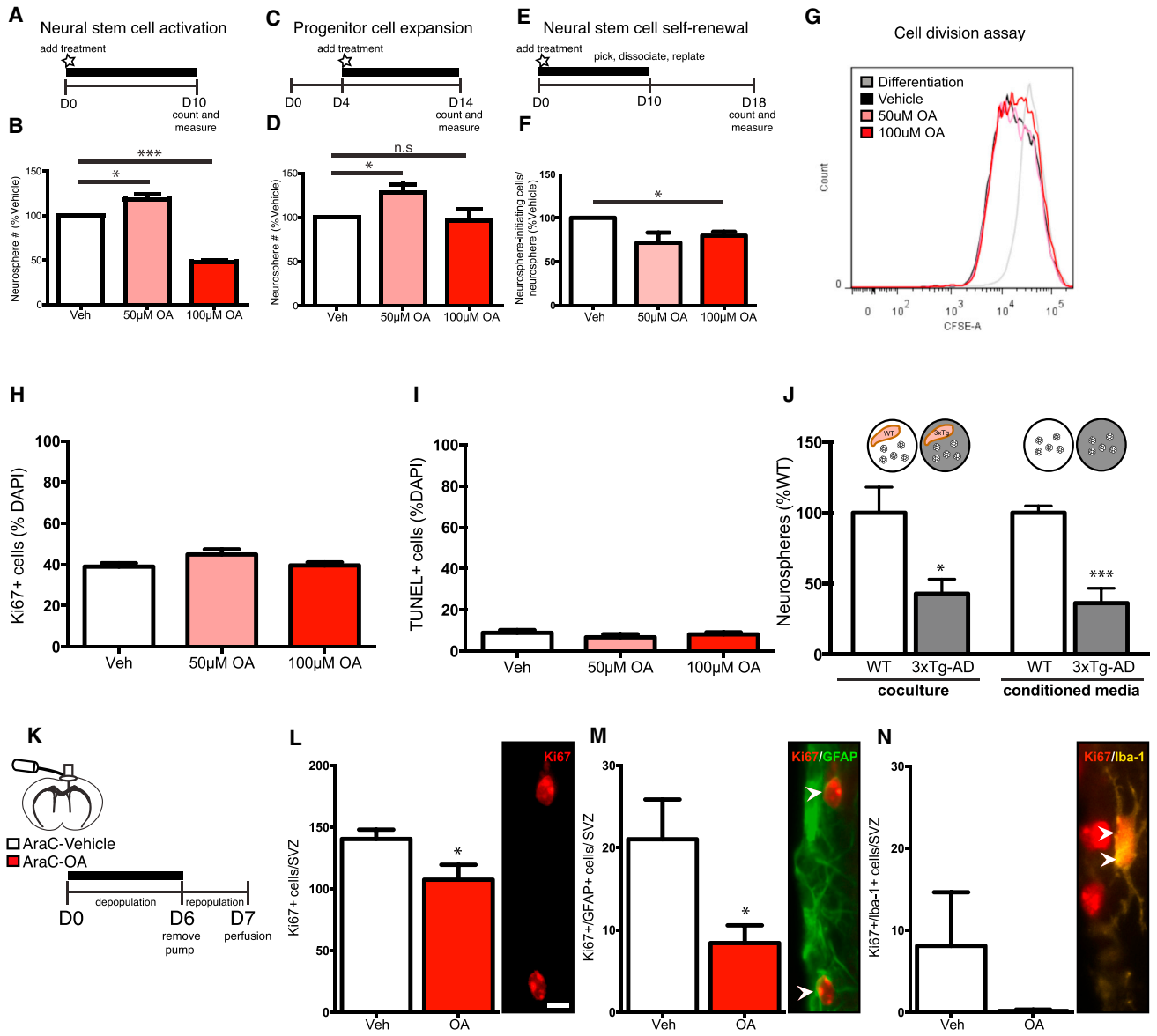

Figure 4. OA Treatment Selectively Suppresses NSC Activity In Vitro and In Vivo

(A–D) Primary neurospheres from C57BL6 mice were dissociated and re-plated under neurosphere-forming conditions and treated with either vehicle or OA (50 or 100 μM) on the day of plating (D0, NSC activation) (A and B) or 4 days later (D4, progenitor expansion) (C and D) (n = 3 per condition). One-way ANOVA.

(E and F) NSC self-renewal was assessed in dissociated secondary neurospheres plated in identical conditions after 10 days of continuous treatment with OA or vehicle (n = 6 per condition). One-way ANOVA.

(G) Dissociated primary neurospheres from C57BL6 mice plated in the presence of EGF and treated on the day of plating with vehicle or 50 or 100 μM OA conjugated to the vehicle for 2–3 days (n = 3 per condition). Quantification by flow cytometry analysis of carboxyfluorescein diacetate succinimidyl ester (CFSE), a cell division assay. Cells were differentiated without EGF as a positive control for differentiation. One-way ANOVA.

(H and I) Quantification of immunocytochemistry for Ki67 (proliferation) (H) and terminal deoxynucleotidyl transferase deoxyuridine triphosphate nick end labeling (TUNEL, cell death) (I) (n = 3 per condition). One-way ANOVA.

(J) Neurosphere growth in the presence of 3xTg-AD or WT SVZ whole mounts (co-culture) (n = 4) or in the presence of filtered conditioned media from 3xTg-AD (n = 3) or WT (n = 5) whole mounts (conditioned media). Unpaired t test.

(K–N) ICV infusion of AraC with vehicle (n = 3) or OA (n = 4). Schematic of AraC SVZ regeneration assay (K) with quantification and representative micrographs of Ki67+ proliferating cells (L), Ki67+/GFAP+ proliferating NSCs (M), and Ki67+/Iba-1+ proliferating microglia (N) in the SVZ. Unpaired t test. Scale bars in (L) (for L–N) represent 5 μm. *$p \leq 0.05$ and ***$p \leq 0.0005$.

See also Figure S3.

infusion in the EV group resulted in a 37.6% decrease in EYFP+ cells relative to vehicle that approached statistical significance ($p = 0.08$) (Figure 6I). Importantly, this OA-induced suppression of NSC proliferative expansion was attenuated in the KD-AKT group (Figure 6I), which exhibited only a 21.2% decrease relative to vehicle ($p = 0.2$). Together, these in vitro and in vivo rescue

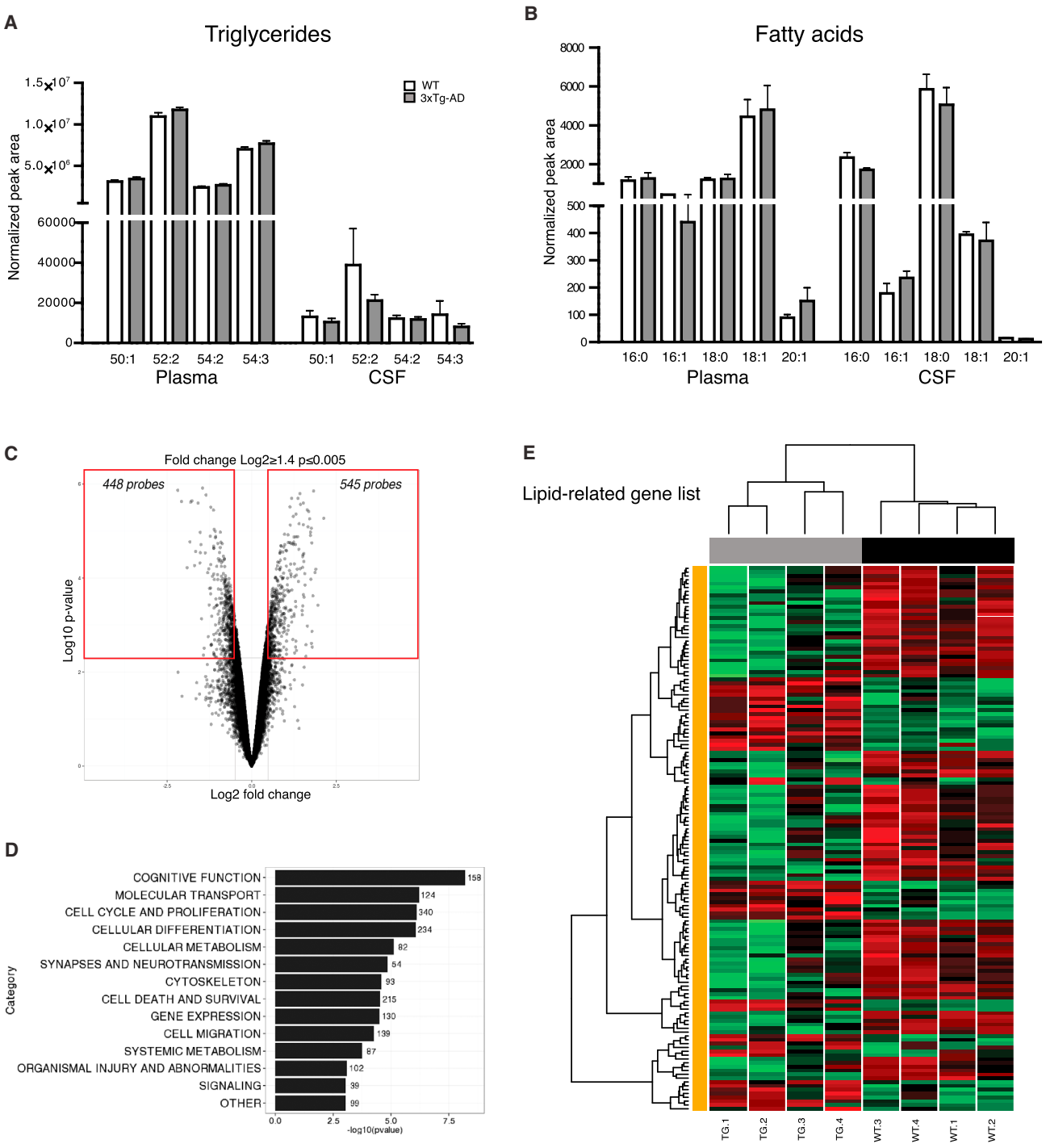

Figure 5. Lipid Metabolism Is Altered within the SVZ of 3xTg-AD Mice

(A and B) LC-MS analysis of lipid species within plasma and CSF of WT and 3xTg-AD mice (n = 4). The normalized peak area for the four major AD-associated triglycerides (A) and their associated fatty acids (B) shows no significant differences. Unpaired t test.

(C–E) Microarray of microdissected SVZs of 7-month-old WT and 3xTg-AD mice (n = 4). (C) Volcano plot. (D) Ingenuity pathway analysis of differentially regulated categories, hand-curated into thematic categories. (E) Heatmap of differentially regulated lipid-related genes, grouped hierarchically. Lipid-related genes were extracted from the list of 993 modulated genes manually and cross-referenced with the Gene Ontology terms lipid, lipoprotein, triglyceride, and fatty acid. Error bars represent mean ± SEM.

See also Figures S4 and S5 and Tables S2 and S3.

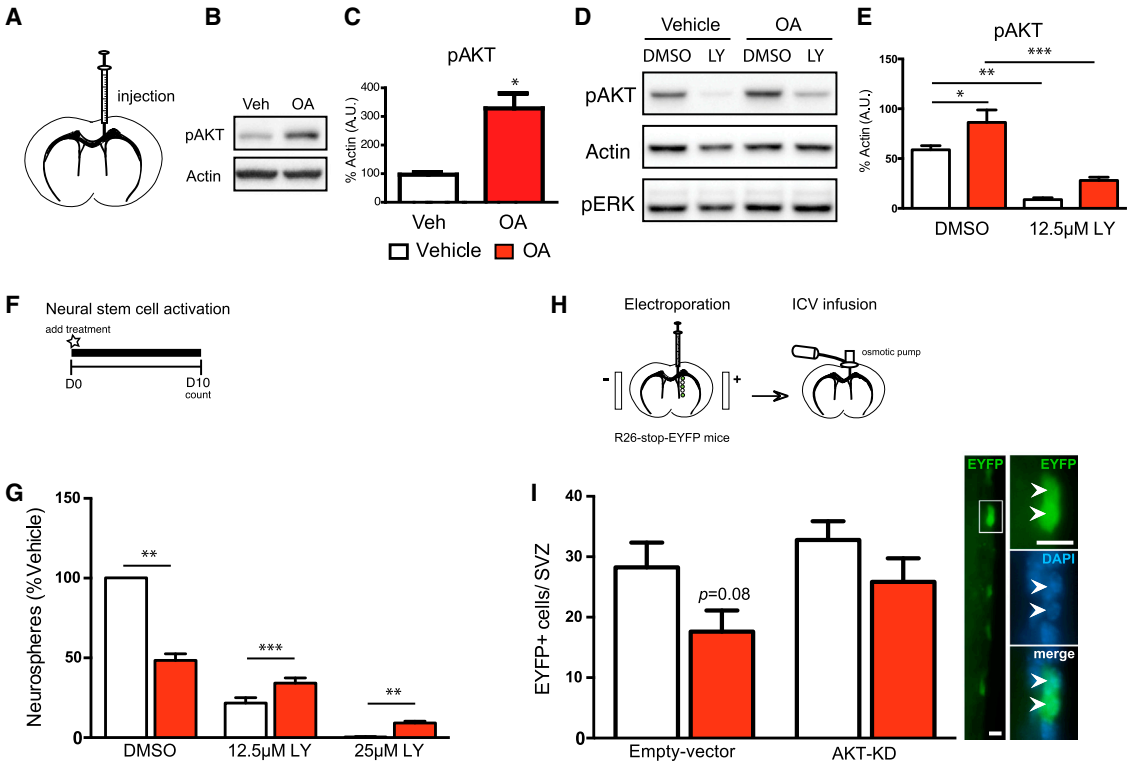

Figure 6. Hyper-Activation of AKT Signaling Mediates OA-Induced Impairment of NSC Activity

(A–C) Acute regulation of the AKT signaling pathway by OA in vivo. Representative western blot of ipsilateral SVZ microdissections 4 hr after ICV injection of vehicle (n = 4) or OA (n = 4) (B) with densitometric quantification of pAKT (C). Unpaired t test.

(D and E) Dissociated primary neurospheres from C57BL6 mice plated and grown in the presence of EGF for 2 days and acutely treated for 4 hr with either vehicle or 100 μM OA alone or combined with 12.5 μM of LY294002 (n = 3). Representative western blot (D) and densitometric quantifications for pAKT (E). One-way ANOVA.

(F and G) Neurospheres grown in the presence of vehicle or 100 μM OA alone or combined with 12.5 or 25 μM of LY294002 (n = 4). Paired t test.

(H and I) Electroporation of a plasmid encoding GFAP-cre into the ventricle walls of adult R26-flox-stop-flox-EYFP mice to induce the expression of EYFP in GFAP+ NSCs and their progeny. The GFAP-cre plasmid was co-electroporated with plasmids overexpressing either KD-AKT or EV. Immediately following electroporation, 7-day osmotic pumps were implanted for ICV infusion of either vehicle or OA (n = 6 animals per condition). Quantification and representative micrograph of the number of EYFP+ cells per ventricle, providing a measure of the proliferative expansion of the electroporated GFAP+ NSCs (I). Unpaired t test. Scale bars in (I) represent 25 μm. Error bars represent mean ± SEM. *p ≤ 0.05, **p ≤ 0.005, and ***p ≤ 0.0005.

experiments provide evidence that exogenous OA suppresses NSC activity via hyper-activation of AKT signaling.

Inhibition of SCD-1 Activity Rescues NSC Impairment in 3xTg-AD Mice

To establish whether NSC suppression in 3xTg-AD mice is due to elevated endogenous OA levels, we tested whether pharmacological inhibition of the OA-producing enzyme, stearoyl-CoA desaturase (SCD), could attenuate the NSC dysfunction. SCD-1 was identified in our microarray analysis of the 3xTg-AD SVZ and is increased in the brains of human AD patients, where levels of SCD-1-derived unsaturated fatty acids correlate negatively with memory performance (Astarita et al., 2011; Cunnane et al., 2012; Fraser et al., 2010). Thus, SCD-1 represents a mechanistically relevant target for NSC modulation in AD.

28-day ICV mini-osmotic pumps containing either vehicle or SCD-1 inhibitor ab142089 were implanted into 3xTg-AD mice at 2 months of age (i.e., the onset of NSC impairments in the SVZ). Analysis of brain sections of these mice by IMS confirmed that infusion of the SCD-1 inhibitor resulted in a generalized reduction of the OA-enriched AD-associated triglycerides in the SVZ (Figure 7A). Remarkably, stage-specific neurogenesis analysis (Figures 7B–7E) revealed that SCD-1 inhibition prevented the decline in the total number of Ki67+ proliferating cells (Figure 7B) and in the Ki67+/GFAP+ NSC subpopulation (Figure 7C) in the SVZ of these 3xTg-AD mice, maintaining levels found in WT animals. Proliferating and total DCX+ neuroblast populations were not decreased in these mice (Figures 7D and 7E). SCD inhibition also caused a small increase in proliferating Iba1+ microglia in both WT and 3xTg-AD mice (WT, 0.0; 3xTg-AD, 3.22 ± 1.834 for vehicle versus WT, 30.07 ± 8.926; 3xTg-AD, 16.47 ± 4.92 cells/SVZ for inhibitor). We also analyzed the DG niche of these mice (which is more distant from the ICV infusion site) and found a complete rescue of total cell proliferation (Figure 7F) and proliferating neuroblasts (Figure 7H), a partial rescue of NSC activity (Figure 7G) and total neuroblasts (Figure 7I), and no change in proliferating microglia (data not shown). This in vivo rescue experiment directly implicates aberrant OA metabolism in AD-associated NSC dysfunction, confirming the central hypothesis of this study and identifying a strategy for rescuing NSC activity in AD.

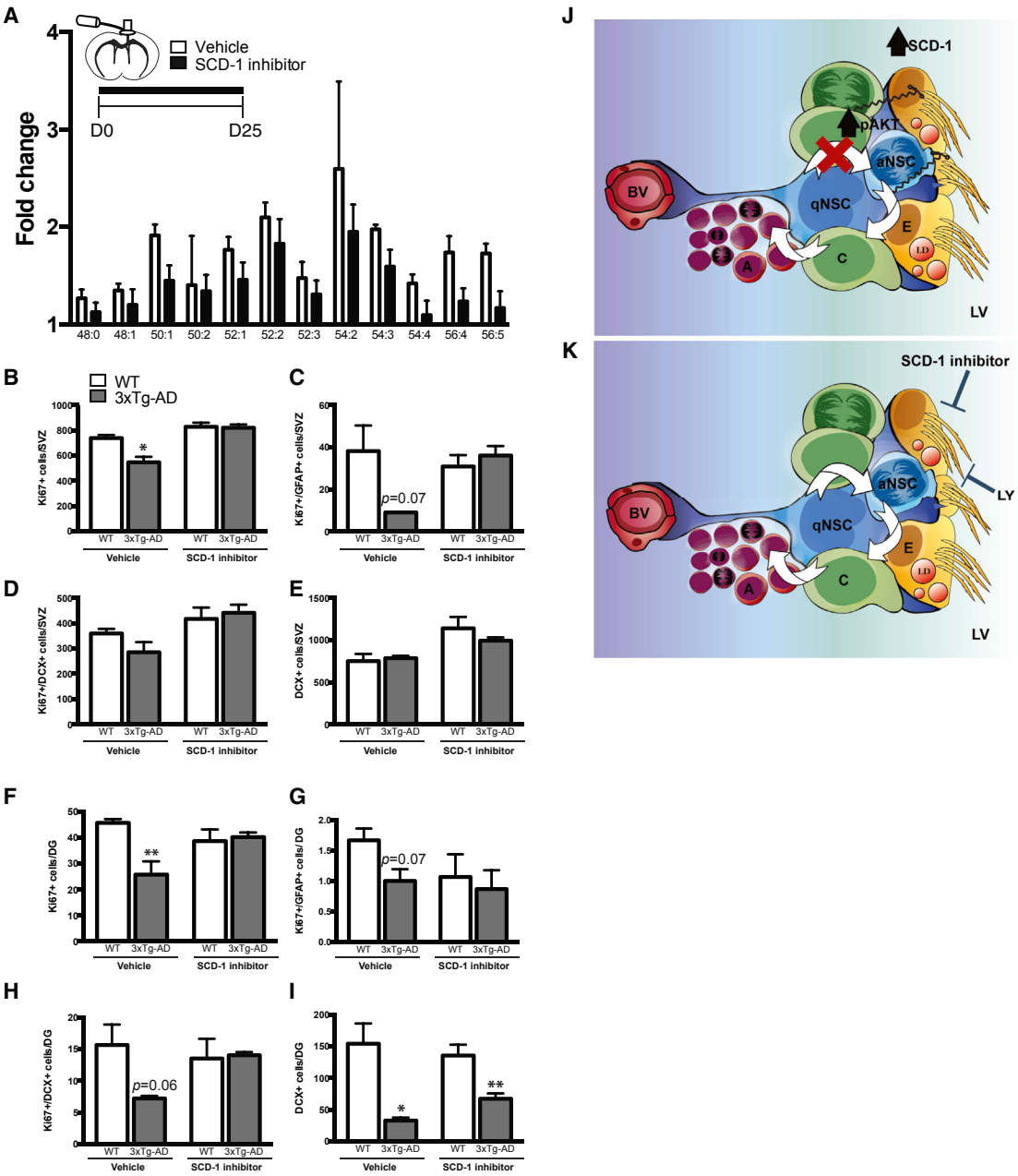

Figure 7. Inhibition of SCD-1 Activity In Vivo Counteracts NSC Impairment in 3xTg-AD Mice

(A) Cohorts of 2-month-old WT or 3xTg-AD mice were implanted with ICV osmotic pumps containing either vehicle (n = 3) or SCD-1 inhibitor (n = 5) for 25 days. The fold change summary of IMS on brain sections shows that SCD-1 inhibitor decreased the accumulation of AD-associated OA-enriched triglycerides in the SVZ.

(B–E) Quantification of Ki67+ proliferating cells (B), Ki67+/GFAP+ proliferating NSCs (C), Ki67+/DCX+ proliferating neuroblasts (D), and DCX+ neuroblasts (E) in the SVZ. Unpaired t test.

(F–I) Quantification of Ki67+ proliferating cells (F), Ki67+/GFAP+ proliferating NSCs (G), Ki67+/DCX+ proliferating neuroblasts (H), and DCX+ neuroblasts (I) in the DG. Unpaired t test.

(J and K) Summary figure. (J) Elevated OA-enriched triglycerides within ependymal cells of 3xTg-AD mice leads to inhibition of NSC proliferation by OA-induced hyper-activation of AKT signaling. (K) Pharmacological inhibition of hyper-activated AKT signaling using a PI3K inhibitor (LY) or inhibition of SCD-1 alleviates OA's inhibitory effects on NSC activation and increases proliferation and neurogenesis. Error bars represent mean ± SEM. *$p \leq 0.05$ and **$p \leq 0.005$.

DISCUSSION

We identified lipid metabolism abnormalities within the NSC niche of AD mice and patients and used recently developed methodologies to dissect their impact on NSC activity. Our results reveal a mechanism of stem cell dysregulation in which disease-induced perturbations of niche fatty acid metabolism suppress adult NSC activity. Moreover, they provide new

support for the notion that AD is, at least in part, a metabolic disease of the brain.

Niche Lipid Metabolism: A Regulator of NSCs

The complexity of identifying and localizing individual brain lipid species represents a major obstacle to deciphering the roles of specific lipids under normal and pathological conditions. Under normal conditions, SVZ neural precursors depend on fatty acid oxidation for proliferation (Stoll et al., 2015), while baseline and exercise-induced hippocampal neurogenesis and cognitive enhancement require brain fatty acid synthesis (Chorna et al., 2013; Knobloch et al., 2013). However, alterations in lipid metabolism are associated with many cognitive disorders, including Huntington's, Parkinson's, and Niemann-Pick's diseases, as well as AD (Adibhatla and Hatcher, 2008; de la Monte and Tong, 2014; Guschina et al., 2011; Martinez-Vicente et al., 2010; Merlo et al., 2010; Sharon et al., 2003). Using imaging techniques, we identified 12 triglycerides that are associated with lipid droplet accumulations in AD, that are enriched with OA side chains, and that selectively accumulate in ependymal cells of the SVZ niche. This accumulation occurred in the absence of changes in circulating triglycerides or fatty acids in either plasma or CSF. However, it was associated with extensive changes in local lipid metabolism gene expression within the SVZ, including in the OA-producing enzyme SCD, which is prominently expressed in peri-ventricular cells (Polo-Hernández et al., 2010; Polo-Hernández et al., 2014). Local OA elevation was sufficient to recapitulate the AD-associated triglyceride profile and selectively suppress NSC expansion in vitro and in vivo. Mechanistically, OA hyper-stimulated the critical AKT-signaling pathway involved in long-term NSC preservation. NSC proliferation impairments could be rescued (1) by inhibiting AKT hyperactivation (with kinase-dead AKT) in OA-treated WT mice or (2) by suppressing endogenous OA synthesis (with an SCD inhibitor) in 3xTg-AD mice. Thus, like many other niche signals, specific fatty acids produced within the NSC niche can influence NSC maintenance via regulation of NSC activation, quiescence, or both.

Implications for the Pathogenesis of Alzheimer's Disease

Neurogenesis occurs in both the human SVZ and the human hippocampus (Ernst and Frisén, 2015). In other vertebrates, hippocampal neurogenesis has been implicated in learning, memory, and mood regulation, and it is likely to have an analogous role in modulating function of the human hippocampus (Spalding et al., 2013). However, human SVZ neurogenesis exhibits a marked evolutionary divergence. Long-distance migration of SVZ-derived neuroblasts to the adult human olfactory bulbs is virtually non-existent (Bergmann et al., 2012), while neurogenesis in the SVZ-adjacent striatum is significantly increased (Ernst et al., 2014). Interestingly, the human striatum has profuse connections with the cortex, and the emergence of human striatal neurogenesis parallels the evolutionarily increased importance of this structure in higher cognitive functions such as cognitive flexibility and mesolimbic functions associated with regulation of reward, motivation, and pleasure (Bergmann et al., 2015).

Our data lead to the predictions that abnormalities in brain lipid metabolism suppress neurogenesis early during pathogenesis of human AD and that this suppression contributes to striatal and hippocampal dysfunction. Consistent with these ideas, atrophy of the hippocampus is a well-established occurrence in AD, and recent analyses of the deep brain gray matter have revealed that striatal abnormalities are more prominent than previously appreciated. Changes to the gross structure and size of the striatum occur early during progression of both familial (early onset) and more common sporadic (late onset) forms of AD (Cho et al., 2013; de Jong et al., 2011; de Jong et al., 2008; Pievani et al., 2013). Indeed, brain imaging has revealed that structural changes of both the striatum and the hippocampus are evident at pre- and early-symptomatic stages in carriers of familial AD-causing mutations (Cash et al., 2013; Lee et al., 2013; Ryan et al., 2013) and that the striatum in particular is the site of the earliest amyloid accumulations in familial AD (Klunk et al., 2007; Knight et al., 2011). In view of the major roles of the human striatum and hippocampus in higher cognition, testing the hypothesis that neurogenesis defects contribute to the early striatal and hippocampal changes occurring in human AD represents an important challenge. This will require the development of innovative diagnostic and imaging tools that can allow in vivo measurement of neurogenesis and ependymal fatty acid levels with high spatial resolution in pre-AD individuals.

Because the hippocampal NSC niche does not directly contact ependymal cells, the partial normalization of hippocampal neurogenesis in 3xTg-AD mice treated with SCD inhibitor suggests that accumulating ependymal lipids penetrate deeper into the brain parenchyma. In this regard, the principal genetic risk factor for sporadic AD is the ApoE4 polymorphism of ApoE, the main lipid transporting apolipoprotein produced in the brain. Inheritance of a single ApoE4 allele increases AD risk by a factor of 4, and two ApoE4 alleles increase the risk by a factor of 20 (Corder et al., 1994; Corder et al., 1993; Strittmatter and Roses, 1996). Furthermore, ApoE polymorphism affects adult neurogenesis (Levi and Michaelson, 2007; Li et al., 2009; Yang et al., 2011). It will therefore be of great interest to know whether the lipid metabolism changes in the SVZ niche have more widespread effects on other aspects of AD pathogenesis, such as gliosis, amyloid plaques, neurofibrillary tangles, cerebrovascular amyloidosis, or synaptic dysfunction.

Collectively, this work shows that excessive levels of OA at the ependymal surface of the brain result in the deterioration of neurogenic niches in AD. Besides directly contributing to cognitive decline, the observed suppression of NSC activity may explain why the brain's stem cell system does not mount a more robust protective or regenerative response in AD. Future work focused on fatty acid metabolism within the brain may lead to new therapeutic approaches to prevent cognitive decline and improve stem cell-mediated brain repair during AD.

EXPERIMENTAL PROCEDURES

Experiments were conducted in accordance with the guidelines of the Canadian Council of Animal Care and were approved by the institutional animal care committee of the Research Center of the University of Montreal Hospital.

Mouse Strains

Female 3xTg-AD $PS1_{M146V}$, APP_{Swe}, and Tau_{P301L}; their littermate WT strain (Oddo et al., 2003); and male C57BL6 mice were used in this study.

ICV Infusions

Alzet osmotic pumps (Durect) were stereotaxically implanted according to manufacturer's instructions. Pumps contained vehicle (fatty acid-free BSA), 500 μM OA, 10 mM ^{12}C OA conjugated to vehicle, or 10 mM ^{13}C OA conjugated to vehicle (the latter for metabolic labeling studies). 2% AraC was ICV infused with vehicle or 500 μM OA for 6 days, pumps were cut out, and mice sacrificed 24 hr later. Vehicle or 40 μM SCD-1 inhibitor was ICV infused for 25 days in 2-month-old WT or 3xTg-AD mice.

ICV Acute Injections

A 10-μl Hamilton syringe was used to inject 2 μl (1 μl/min) of vehicle or 500 μM OA into the lateral ventricle of C57BL6 mice. Mice were sacrificed 4 hr later.

Adult Brain Electroporations

Electroporations were performed as described (Barnabé-Heider et al., 2008). Plasmids were stereotaxically injected into the left lateral ventricle (coordinates: 0-mm anterior-posterior, 0.9-mm medial-lateral, and 1.5-mm dorsoventral, relative to Bregma). Each animal received an ICV injection of 2 μl, delivered over 1.5–2 min, containing 10 μg of each plasmid (20 μg total). Human GFAP-cre (Michael Brenner, Raul Torres, and Klaus Rajewsky, cat# 40591, Addgene) with either KD-AKT (AKT-K179N) (William Sellers, cat# 9007, Addgene) or pECE EV (William Rutter, cat# 26453, Addgene) plasmids was co-electroporated.

Neurosphere Assays

Neurospheres were generated using 20 ng/ml of epidermal growth factor (EGF) (Sigma) as described previously (Bouab et al., 2011), according to a procedure modified from Reynolds and Weiss (1992). Clonal neurospheres were grown at a density of 1.5 cells/μl in 24-well plates.

Laser Desorption Ionization Imaging Mass Spectrometry and Tandem Mass Spectrometry

Spectral acquisitions were performed on either a MALDI-TOF/TOF Ultraflextreme mass spectrometer equipped with a SmartBeam II Nd:YAG/355-nm laser or a SolariX XR 7T ParaCell Fourier transform ion cyclotronic resonance (FT-ICR). IMS data were acquired using 100 shots per pixel using a 10-μm lateral resolution and with a spectral resolution of 80,000 μm at a mass-to-charge (m/z) ratio of 881.7569.

LC-MS

Plasma and CSF lipid extractions were carried out on a Synapt G2-S instrument coupled to an Acquity UPLC Class I system both from waters.

Microarray

Microdissected SVZs from 7-month-old WT and 3xTg-AD mice were hybridized to the SurePrint G3 Mouse GE 8×60K microarray (Agilent Technologies). Microarray data are deposited in the GEO under accession number GEO: GSE60460.

Statistical Analysis

Two-tailed unpaired t test, paired Student's t test, or one-way ANOVA with Tukey post hoc test was used as indicated in figure legends. All error bars represent mean ± SEM. The significance level was set at $p \leq 0.05$.

SUPPLEMENTAL INFORMATION

Supplemental Information includes Supplemental Experimental Procedures, five figures, and three tables and can be found with this article online at http://dx.doi.org/10.1016/j.stem.2015.08.001.

AUTHOR CONTRIBUTIONS

L.K.H. developed the concept, carried out experiments, analyzed data, and co-wrote the paper. M.D. and P.C. developed and carried out IMS experiments and analyzed data. S.E.J. contributed to neurogenesis experiments and flow cytometry. S.P. and M.P. carried out the human studies. A.A. contributed to neurogenesis experiments. F.B.-H. provided expertise with the in vivo electroporations. A.F. performed the LC-MS experiments and analyzed data. F.C. provided the 3xTg-AD mice. K.J.L.F. developed the concept, performed surgeries, analyzed data, and co-wrote the paper. All authors revised the manuscript.

ACKNOWLEDGMENTS

We thank Dr. S. Lacroix and N. Fortin for CSF and plasma extractions; Bruker Daltonics for access to the FT-ICR; K. Kellersberger for assistance with all FT-ICR-related data acquisition; the Genomics platform at The Institute for Research on Immunology and Cancer (IRIC) for microarray and bio-informatics analyses; and D. Gauchat at the CRCHUM cytometry core facility for assistance with flow cytometry. L.K.H. is funded by studentships from the Alzheimer Society of Canada and the Fonds de recherche de Québec en Santé (FRQS). K.J.L.F. holds a Canada Research Chair in neural stem cell biology. This work has been supported by the Canadian Institutes of Health Research (CIHR).

Received: October 5, 2014
Revised: June 9, 2015
Accepted: August 2, 2015
Published: August 27, 2015

REFERENCES

Adibhatla, R.M., and Hatcher, J.F. (2008). Altered lipid metabolism in brain injury and disorders. Subcell. Biochem. *49*, 241–268.

Alzheimer, A. (1907). Über eine eigenartige erkrankung der hirnrinde. Allgemeine Zeitschrift für Psychiatrie und psychisch-gerichtliche Medizin *64*, 146–148.

Astarita, G., Jung, K.M., Vasilevko, V., Dipatrizio, N.V., Martin, S.K., Cribbs, D.H., Head, E., Cotman, C.W., and Piomelli, D. (2011). Elevated stearoyl-CoA desaturase in brains of patients with Alzheimer's disease. PLoS ONE *6*, e24777.

Barnabé-Heider, F., Meletis, K., Eriksson, M., Bergmann, O., Sabelström, H., Harvey, M.A., Mikkers, H., and Frisén, J. (2008). Genetic manipulation of adult mouse neurogenic niches by in vivo electroporation. Nat. Methods *5*, 189–196.

Benner, E.J., Luciano, D., Jo, R., Abdi, K., Paez-Gonzalez, P., Sheng, H., Warner, D.S., Liu, C., Eroglu, C., and Kuo, C.T. (2013). Protective astrogenesis from the SVZ niche after injury is controlled by Notch modulator Thbs4. Nature *497*, 369–373.

Bergmann, O., Liebl, J., Bernard, S., Alkass, K., Yeung, M.S., Steier, P., Kutschera, W., Johnson, L., Landén, M., Druid, H., et al. (2012). The age of olfactory bulb neurons in humans. Neuron *74*, 634–639.

Bergmann, O., Spalding, K.L., and Frisén, J. (2015). Adult neurogenesis in humans. Cold Spring Harb. Perspect. Biol. *7*, 1–12.

Bouab, M., Paliouras, G.N., Aumont, A., Forest-Bérard, K., and Fernandes, K.J. (2011). Aging of the subventricular zone neural stem cell niche: evidence for quiescence-associated changes between early and mid-adulthood. Neuroscience *173*, 135–149.

Cash, D.M., Ridgway, G.R., Liang, Y., Ryan, N.S., Kinnunen, K.M., Yeatman, T., Malone, I.B., Benzinger, T.L., Jack, C.R., Jr., Thompson, P.M., et al.; Dominantly Inherited Alzheimer Network (DIAN) (2013). The pattern of atrophy in familial Alzheimer disease: volumetric MRI results from the DIAN study. Neurology *81*, 1425–1433.

Cho, H., Seo, S.W., Kim, J.H., Kim, C., Ye, B.S., Kim, G.H., Noh, Y., Kim, H.J., Yoon, C.W., Seong, J.K., et al. (2013). Changes in subcortical structures in early- versus late-onset Alzheimer's disease. Neurobiol. Aging *34*, 1740–1747.

Chorna, N.E., Santos-Soto, I.J., Carballeira, N.M., Morales, J.L., de la Nuez, J., Cátala-Valentin, A., Chornyy, A.P., Vázquez-Montes, A., and De Ortiz, S.P. (2013). Fatty acid synthase as a factor required for exercise-induced cognitive enhancement and dentate gyrus cellular proliferation. PLoS ONE *8*, e77845.

Chuang, T.T. (2010). Neurogenesis in mouse models of Alzheimer's disease. Biochim. Biophys. Acta *1802*, 872–880.

Codega, P., Silva-Vargas, V., Paul, A., Maldonado-Soto, A.R., Deleo, A.M., Pastrana, E., and Doetsch, F. (2014). Prospective identification and purification of quiescent adult neural stem cells from their in vivo niche. Neuron *82*, 545–559.

Corder, E.H., Saunders, A.M., Strittmatter, W.J., Schmechel, D.E., Gaskell, P.C., Small, G.W., Roses, A.D., Haines, J.L., and Pericak-Vance, M.A. (1993). Gene dose of apolipoprotein E type 4 allele and the risk of Alzheimer's disease in late onset families. Science *261*, 921–923.

Corder, E.H., Saunders, A.M., Risch, N.J., Strittmatter, W.J., Schmechel, D.E., Gaskell, P.C., Jr., Rimmler, J.B., Locke, P.A., Conneally, P.M., Schmader, K.E., et al. (1994). Protective effect of apolipoprotein E type 2 allele for late onset Alzheimer disease. Nat. Genet. *7*, 180–184.

Crews, L., Adame, A., Patrick, C., Delaney, A., Pham, E., Rockenstein, E., Hansen, L., and Masliah, E. (2010). Increased BMP6 levels in the brains of Alzheimer's disease patients and APP transgenic mice are accompanied by impaired neurogenesis. J. Neurosci. *30*, 12252–12262.

Cunnane, S.C., Schneider, J.A., Tangney, C., Tremblay-Mercier, J., Fortier, M., Bennett, D.A., and Morris, M.C. (2012). Plasma and brain fatty acid profiles in mild cognitive impairment and Alzheimer's disease. J. Alzheimers Dis. *29*, 691–697.

de Chevigny, A., Cooper, O., Vinuela, A., Reske-Nielsen, C., Lagace, D.C., Eisch, A.J., and Isacson, O. (2008). Fate mapping and lineage analyses demonstrate the production of a large number of striatal neuroblasts after transforming growth factor alpha and noggin striatal infusions into the dopamine-depleted striatum. Stem Cells *26*, 2349–2360.

de Jong, L.W., van der Hiele, K., Veer, I.M., Houwing, J.J., Westendorp, R.G., Bollen, E.L., de Bruin, P.W., Middelkoop, H.A., van Buchem, M.A., and van der Grond, J. (2008). Strongly reduced volumes of putamen and thalamus in Alzheimer's disease: an MRI study. Brain *131*, 3277–3285.

de Jong, L.W., Ferrarini, L., van der Grond, J., Milles, J.R., Reiber, J.H., Westendorp, R.G., Bollen, E.L., Middelkoop, H.A., and van Buchem, M.A. (2011). Shape abnormalities of the striatum in Alzheimer's disease. J. Alzheimers Dis. *23*, 49–59.

de la Monte, S.M., and Tong, M. (2014). Brain metabolic dysfunction at the core of Alzheimer's disease. Biochem. Pharmacol. *88*, 548–559.

Demars, M., Hu, Y.S., Gadadhar, A., and Lazarov, O. (2010). Impaired neurogenesis is an early event in the etiology of familial Alzheimer's disease in transgenic mice. J. Neurosci. Res. *88*, 2103–2117.

Doetsch, F., García-Verdugo, J.M., and Alvarez-Buylla, A. (1997). Cellular composition and three-dimensional organization of the subventricular germinal zone in the adult mammalian brain. J. Neurosci. *17*, 5046–5061.

Doetsch, F., García-Verdugo, J.M., and Alvarez-Buylla, A. (1999). Regeneration of a germinal layer in the adult mammalian brain. Proc. Natl. Acad. Sci. USA *96*, 11619–11624.

Erlandsson, A., Lin, C.H., Yu, F., and Morshead, C.M. (2011). Immunosuppression promotes endogenous neural stem and progenitor cell migration and tissue regeneration after ischemic injury. Exp. Neurol. *230*, 48–57.

Ernst, A., and Frisén, J. (2015). Adult neurogenesis in humans—common and unique traits in mammals. PLoS Biol. *13*, e1002045.

Ernst, A., Alkass, K., Bernard, S., Salehpour, M., Perl, S., Tisdale, J., Possnert, G., Druid, H., and Frisén, J. (2014). Neurogenesis in the striatum of the adult human brain. Cell *156*, 1072–1083.

Etschmaier, K., Becker, T., Eichmann, T.O., Schweinzer, C., Scholler, M., Tam-Amersdorfer, C., Poeckl, M., Schuligoi, R., Kober, A., Chirackal Manavalan, A.P., et al. (2011). Adipose triglyceride lipase affects triacylglycerol metabolism at brain barriers. J. Neurochem. *119*, 1016–1028.

Fraser, T., Tayler, H., and Love, S. (2010). Fatty acid composition of frontal, temporal and parietal neocortex in the normal human brain and in Alzheimer's disease. Neurochem. Res. *35*, 503–513.

Guschina, I., Millership, S., O'Donnell, V., Ninkina, N., Harwood, J., and Buchman, V. (2011). Lipid classes and fatty acid patterns are altered in the brain of γ-synuclein null mutant mice. Lipids *46*, 121–130.

Hamilton, L.K., Aumont, A., Julien, C., Vadnais, A., Calon, F., and Fernandes, K.J. (2010). Widespread deficits in adult neurogenesis precede plaque and tangle formation in the 3xTg mouse model of Alzheimer's disease. Eur. J. Neurosci. *32*, 905–920.

Hamilton, L.K., Joppé, S.E., Cochard, L.M., and Fernandes, K.J.L. (2013). Aging and neurogenesis in the adult forebrain: what we have learned and where we should go from here. Eur. J. Neurosci. *37*, 1978–1986.

Hussain, G., Schmitt, F., Loeffler, J.P., and Gonzalez de Aguilar, J.L. (2013). Fatting the brain: a brief of recent research. Front. Cell. Neurosci. *7*, 144.

Imayoshi, I., Sakamoto, M., Ohtsuka, T., Takao, K., Miyakawa, T., Yamaguchi, M., Mori, K., Ikeda, T., Itohara, S., and Kageyama, R. (2008). Roles of continuous neurogenesis in the structural and functional integrity of the adult forebrain. Nat. Neurosci. *11*, 1153–1161.

Klunk, W.E., Price, J.C., Mathis, C.A., Tsopelas, N.D., Lopresti, B.J., Ziolko, S.K., Bi, W., Hoge, J.A., Cohen, A.D., Ikonomovic, M.D., et al. (2007). Amyloid deposition begins in the striatum of presenilin-1 mutation carriers from two unrelated pedigrees. J. Neurosci. *27*, 6174–6184.

Knight, W.D., Okello, A.A., Ryan, N.S., Turkheimer, F.E., Rodríguez Martinez de Llano, S., Edison, P., Douglas, J., Fox, N.C., Brooks, D.J., and Rossor, M.N. (2011). Carbon-11-Pittsburgh compound B positron emission tomography imaging of amyloid deposition in presenilin 1 mutation carriers. Brain *134*, 293–300.

Knobloch, M., Braun, S.M., Zurkirchen, L., von Schoultz, C., Zamboni, N., Araúzo-Bravo, M.J., Kovacs, W.J., Karalay, O., Suter, U., Machado, R.A., et al. (2013). Metabolic control of adult neural stem cell activity by Fasn-dependent lipogenesis. Nature *493*, 226–230.

Kolb, B., Morshead, C., Gonzalez, C., Kim, M., Gregg, C., Shingo, T., and Weiss, S. (2007). Growth factor-stimulated generation of new cortical tissue and functional recovery after stroke damage to the motor cortex of rats. J. Cereb. Blood Flow Metab. *27*, 983–997.

Lazarov, O., and Marr, R.A. (2010). Neurogenesis and Alzheimer's disease: at the crossroads. Exp. Neurol. *223*, 267–281.

Lazarov, O., Mattson, M.P., Peterson, D.A., Pimplikar, S.W., and van Praag, H. (2010). When neurogenesis encounters aging and disease. Trends Neurosci. *33*, 569–579.

Lee, G.J., Lu, P.H., Medina, L.D., Rodriguez-Agudelo, Y., Melchor, S., Coppola, G., Braskie, M.N., Hua, X., Apostolova, L.G., Leow, A.D., et al. (2013). Regional brain volume differences in symptomatic and presymptomatic carriers of familial Alzheimer's disease mutations. J. Neurol. Neurosurg. Psychiatry *84*, 154–162.

Lee, S.M., Choi, H., Yang, G., Park, K.C., Jeong, S., and Hong, S. (2014). MicroRNAs mediate oleic acid-induced acute lung injury in rats using an alternative injury mechanism. Mol. Med. Rep. *10*, 292–300.

Levi, O., and Michaelson, D.M. (2007). Environmental enrichment stimulates neurogenesis in apolipoprotein E3 and neuronal apoptosis in apolipoprotein E4 transgenic mice. J. Neurochem. *100*, 202–210.

Li, G., Bien-Ly, N., Andrews-Zwilling, Y., Xu, Q., Bernardo, A., Ring, K., Halabisky, B., Deng, C., Mahley, R.W., and Huang, Y. (2009). GABAergic interneuron dysfunction impairs hippocampal neurogenesis in adult apolipoprotein E4 knockin mice. Cell Stem Cell *5*, 634–645.

Martin, S., and Parton, R.G. (2006). Lipid droplets: a unified view of a dynamic organelle. Nat. Rev. Mol. Cell Biol. *7*, 373–378.

Martinez-Vicente, M., Talloczy, Z., Wong, E., Tang, G., Koga, H., Kaushik, S., de Vries, R., Arias, E., Harris, S., Sulzer, D., and Cuervo, A.M. (2010). Cargo recognition failure is responsible for inefficient autophagy in Huntington's disease. Nat. Neurosci. *13*, 567–576.

Matsumata, M., Sakayori, N., Maekawa, M., Owada, Y., Yoshikawa, T., and Osumi, N. (2012). The effects of Fabp7 and Fabp5 on postnatal hippocampal neurogenesis in the mouse. Stem Cells *30*, 1532–1543.

Merlo, S., Spampinato, S., Canonico, P.L., Copani, A., and Sortino, M.A. (2010). Alzheimer's disease: brain expression of a metabolic disorder? Trends Endocrinol. Metab. *21*, 537–544.

Mirzadeh, Z., Merkle, F.T., Soriano-Navarro, M., Garcia-Verdugo, J.M., and Alvarez-Buylla, A. (2008). Neural stem cells confer unique pinwheel architecture to the ventricular surface in neurogenic regions of the adult brain. Cell Stem Cell *3*, 265–278.

Nho, K., Kim, S., Risacher, S.L., Shen, L., Corneveaux, J.J., Swaminathan, S., Lin, H., Ramanan, V.K., Liu, Y., Foroud, T.M., et al.; MIRAGE (Multi-Institutional

Research on Alzheimer Genetic Epidemiology) Study; AddNeuroMed Consortium; Indiana Memory and Aging Study; Alzheimer's Disease Neuroimaging Initiative (2015). Protective variant for hippocampal atrophy identified by whole exome sequencing. Ann. Neurol. *77*, 547–552.

Oddo, S., Caccamo, A., Kitazawa, M., Tseng, B.P., and LaFerla, F.M. (2003). Amyloid deposition precedes tangle formation in a triple transgenic model of Alzheimer's disease. Neurobiol. Aging *24*, 1063–1070.

Pasinetti, G.M., and Eberstein, J.A. (2008). Metabolic syndrome and the role of dietary lifestyles in Alzheimer's disease. J. Neurochem. *106*, 1503–1514.

Perry, E.K., Johnson, M., Ekonomou, A., Perry, R.H., Ballard, C., and Attems, J. (2012). Neurogenic abnormalities in Alzheimer's disease differ between stages of neurogenesis and are partly related to cholinergic pathology. Neurobiol. Dis. *47*, 155–162.

Pievani, M., Bocchetta, M., Boccardi, M., Cavedo, E., Bonetti, M., Thompson, P.M., and Frisoni, G.B. (2013). Striatal morphology in early-onset and late-onset Alzheimer's disease: a preliminary study. Neurobiol. Aging *34*, 1728–1739.

Podtelezhnikov, A.A., Tanis, K.Q., Nebozhyn, M., Ray, W.J., Stone, D.J., and Loboda, A.P. (2011). Molecular insights into the pathogenesis of Alzheimer's disease and its relationship to normal aging. PLoS ONE *6*, e29610.

Polo-Hernández, E., De Castro, F., García-García, A.G., Tabernero, A., and Medina, J.M. (2010). Oleic acid synthesized in the periventricular zone promotes axonogenesis in the striatum during brain development. J. Neurochem. *114*, 1756–1766.

Polo-Hernández, E., Tello, V., Arroyo, A.A., Domínguez-Prieto, M., de Castro, F., Tabernero, A., and Medina, J.M. (2014). Oleic acid synthesized by stearoyl-CoA desaturase (SCD-1) in the lateral periventricular zone of the developing rat brain mediates neuronal growth, migration and the arrangement of prospective synapses. Brain Res. *1570*, 13–25.

Reynolds, B.A., and Weiss, S. (1992). Generation of neurons and astrocytes from isolated cells of the adult mammalian central nervous system. Science *255*, 1707–1710.

Ryan, N.S., Keihaninejad, S., Shakespeare, T.J., Lehmann, M., Crutch, S.J., Malone, I.B., Thornton, J.S., Mancini, L., Hyare, H., Yousry, T., et al. (2013). Magnetic resonance imaging evidence for presymptomatic change in thalamus and caudate in familial Alzheimer's disease. Brain *136*, 1399–1414.

Sakamoto, M., Imayoshi, I., Ohtsuka, T., Yamaguchi, M., Mori, K., and Kageyama, R. (2011). Continuous neurogenesis in the adult forebrain is required for innate olfactory responses. Proc. Natl. Acad. Sci. USA *108*, 8479–8484.

Sakamoto, M., Ieki, N., Miyoshi, G., Mochimaru, D., Miyachi, H., Imura, T., Yamaguchi, M., Fishell, G., Mori, K., Kageyama, R., and Imayoshi, I. (2014). Continuous postnatal neurogenesis contributes to formation of the olfactory bulb neural circuits and flexible olfactory associative learning. J. Neurosci. *34*, 5788–5799.

Sharon, R., Bar-Joseph, I., Frosch, M.P., Walsh, D.M., Hamilton, J.A., and Selkoe, D.J. (2003). The formation of highly soluble oligomers of alpha-synuclein is regulated by fatty acids and enhanced in Parkinson's disease. Neuron *37*, 583–595.

Shibata, E., Kanno, T., Tsuchiya, A., Kuribayashi, K., Tabata, C., Nakano, T., and Nishizaki, T. (2013). Free fatty acids inhibit protein tyrosine phosphatase 1B and activate Akt. Cell. Physiol. Biochem. *32*, 871–879.

Smukler, S.R., Arntfield, M.E., Razavi, R., Bikopoulos, G., Karpowicz, P., Seaberg, R., Dai, F., Lee, S., Ahrens, R., Fraser, P.E., et al. (2011). The adult mouse and human pancreas contain rare multipotent stem cells that express insulin. Cell Stem Cell *8*, 281–293.

Snyder, J.S., Kee, N., and Wojtowicz, J.M. (2001). Effects of adult neurogenesis on synaptic plasticity in the rat dentate gyrus. J. Neurophysiol. *85*, 2423–2431.

Spalding, K.L., Bergmann, O., Alkass, K., Bernard, S., Salehpour, M., Huttner, H.B., Boström, E., Westerlund, I., Vial, C., Buchholz, B.A., et al. (2013). Dynamics of hippocampal neurogenesis in adult humans. Cell *153*, 1219–1227.

Stoll, E.A., Makin, R., Sweet, I.R., Trevelyan, A.J., Miwa, S., Horner, P.J., and Turnbull, D.M. (2015). Neural stem cells in the adult subventricular zone oxidize fatty acids to produce energy and support neurogenic activity. Stem Cells *33*, 2306–2319.

Strittmatter, W.J., and Roses, A.D. (1996). Apolipoprotein E and Alzheimer's disease. Annu. Rev. Neurosci. *19*, 53–77.

Talwar, P., Silla, Y., Grover, S., Gupta, M., Agarwal, R., Kushwaha, S., and Kukreti, R. (2014). Genomic convergence and network analysis approach to identify candidate genes in Alzheimer's disease. BMC Genomics *15*, 199.

Tanzi, R.E. (2012). The genetics of Alzheimer disease. Cold Spring Harb. Perspect. Med. *2*, 1–10.

Tavazoie, M., Van der Veken, L., Silva-Vargas, V., Louissaint, M., Colonna, L., Zaidi, B., Garcia-Verdugo, J.M., and Doetsch, F. (2008). A specialized vascular niche for adult neural stem cells. Cell Stem Cell *3*, 279–288.

Yang, C.P., Gilley, J.A., Zhang, G., and Kernie, S.G. (2011). ApoE is required for maintenance of the dentate gyrus neural progenitor pool. Development *138*, 4351–4362.

Yun, M.R., Lee, J.Y., Park, H.S., Heo, H.J., Park, J.Y., Bae, S.S., Hong, K.W., Sung, S.M., and Kim, C.D. (2006). Oleic acid enhances vascular smooth muscle cell proliferation via phosphatidylinositol 3-kinase/Akt signaling pathway. Pharmacol. Res. *54*, 97–102.

Ziabreva, I., Perry, E., Perry, R., Minger, S.L., Ekonomou, A., Przyborski, S., and Ballard, C. (2006). Altered neurogenesis in Alzheimer's disease. J. Psychosom. Res. *61*, 311–316.